Mon. Not. R. Astron. Soc. **375,** 1269–1279 (2007) doi:10.1111/j.1365-2966.2006.11361.x

Heating of the intergalactic medium by primordial miniquasars

Saleem Zaroubi,[1★] Rajat M. Thomas,[1] Naoshi Sugiyama[2] and Joseph Silk[3]

[1] *Kapteyn Astronomical Institute, University of Groningen, Landleven 12, 9747 AG Groningen, the Netherlands*
[2] *Department of Physics and Astrophysics, Nagoya University, Chikusa-ku Nagoya 464-8602, Japan*
[3] *Astrophysics Department, University of Oxford, Keble Road, Oxford OX1 3RH*

Accepted 2006 November 29. Received 2006 November 29; in original form 2006 September 6

ABSTRACT

A simple analytical model is used to calculate the X-ray heating of the intergalactic medium (IGM) for a range of black hole masses. This process is efficient enough to decouple the spin temperature of the IGM from the cosmic microwave background (CMB) temperature and produce a differential brightness temperature of the order of $\sim$ 5–20 mK out to distances as large as a few comoving Mpc, depending on the redshift, black hole mass and lifetime. We explore the influence of two types of black holes, those with and without ionizing ultraviolet radiation. The results of the simple analytical model are compared to those of a full spherically symmetric radiative transfer code. Two simple scenarios are proposed for the formation and evolution of black hole mass density in the Universe. The first considers an intermediate mass black hole that form as an end-product of pop III stars, whereas the second considers supermassive black holes that form directly through the collapse of massive haloes with low spin parameter. These scenarios are shown not to violate any of the observational constraints, yet produce enough X-ray photons to decouple the spin temperature from that of the CMB. This is an important issue for future high-redshift 21-cm observations.

Key words: quasars: general – cosmology: theory – diffuse radiation – large-scale structure of Universe – radio lines: general.

1 INTRODUCTION

One of the most startling findings made in the last few years is the discovery of supermassive black holes (SMBHs) at redshifts $\gtrsim$5.7 with black hole masses of the order of $10^9\,\mathrm{M}_\odot$ (Fan et al. 2003, 2006). The origin and seeds of these black holes remain uncertain.

Currently, there are two main scenarios for creating such massive black holes. One is as the end-product of the first metal free stars (pop III stars) that have formed through molecular hydrogen cooling (Abel, Bryan & Norman 2000, 2002; Bromm, Coppi & Larson 2002; Yoshida et al. 2003). Given the low cooling rate provided by molecular hydrogen, the collapsing initial cloud is expected not to be able to fragment into small masses and thus produce very massive stars (for reviews, see Bromm & Larson 2004; Ciardi & Ferrara 2005). These stars are expected to burn their fuel very quickly and to produce black holes with masses in the range 30–1000 $\mathrm{M}_\odot$ (O'Shea & Norman 2007), with the exception of the mass range of 140–260 $\mathrm{M}_\odot$ where the pair-instability supernovae leave no black hole remnants (Rakavy, Shaviv & Zinamon 1967; Bond, Arnett & Carr 1984; Heger & Woosley 2002). Such objects grew their masses very efficiently by accretion up to $10^9\,\mathrm{M}_\odot$ by $z \approx 6$ (Volonteri & Rees 2005; Rhook & Haehnelt 2006).

The second avenue for producing even more massive black holes is through the collapse of very low angular momentum gas in rare dark matter haloes with virial temperatures above 10^4 K (see Shapiro 2004 for a recent review). Under such conditions, atomic cooling becomes efficient and black holes with masses $\gg 10^3\,\mathrm{M}_\odot$ can be formed (Bromm & Loeb 2003). Fragmentation of the initial gas into smaller mass objects due to efficient cooling can be prevented by trapping the Lyman α photons within the collapsing gas (Spaans & Silk 2006).

Notwithstanding the origin of these massive black holes, their impact on the intergalactic medium (IGM) is expected to be dramatic in at least two ways. First, these objects produce very intense ionizing radiation with power-law behaviour that creates a different ionization pattern around them from that associated with thermal (i.e. stellar) sources. The ionization aspect of the miniquasar radiation has been explored by several authors (Madau, Meiksin & Rees 1997; Madau et al. 2004; Ricotti & Ostriker 2004a,b; Zaroubi & Silk 2005). Recently, however, it has been argued (Dijkstra, Haiman & Loeb 2004; Salvaterra, Haardt & Ferrara 2005) that miniquasars cannot reionize the Universe as they will produce far more soft X-ray background (SXRB) radiation than currently observed (Moretti et al. 2003; Sołtan 2003) and at the same time satisfy the

★E-mail: saleem@astro.rug.nl

Wilkinson Microwave Anisotropy Probe (*WMAP*) 3rd year polarization results (Page et al. 2006; Spergel et al. 2006) and the reionization constraints from the IGM temperature at redshift ≈3 (Schaye et al. 2000; Theuns et al. 2002a,b). It should be noted, however, that the Dijkstra et al. (2004) and Salvaterra et al. (2005) calculations have been carried out assuming specific black hole mass density evolution histories and spectral energy distributions of ultraviolet (UV)/X-ray radiation emanating from the miniquasars.

Secondly, due to their X-ray radiation, even the intermediate mass black holes (IMBH) are very efficient in heating up their surroundings. Nusser (2005) has pointed out that this heating facilitates observation of the redshifted 21-cm radiation in either emission or absorption by the neutral hydrogen in the high-redshift IGM. The observation of this radiation is controlled by the 21-cm spin temperature, $T_{\rm spin}$, defined through the equation $n_1/n_0 = 3\exp(-T_*/T_{\rm spin})$. Here n_1 and n_0 are the number densities of electrons in the triplet and singlet states of the hyperfine levels, and $T_* = 0.0681$ K is the temperature corresponding to the 21 cm wavelength. For the 21-cm radiation to be observed relative to the cosmic microwave background (CMB), it has to attain a different temperature and therefore must be decoupled from the CMB (Wouthuysen 1952; Field 1958; Field 1959; Hogan & Rees 1979). The decoupling is achieved through either Lyman α radiation or collisional excitations and heating. For the objects we are concerned with in this paper, that is, miniquasars, the collisional excitation and heating are much more important. In general, throughout this paper, we will ignore the influence of Lyman α photons emitted by the quasar on $T_{\rm spin}$. However, one should point out that collisional excitations due to X-ray photons results in a 'secondary' Lyman α pumping which will dominate the spin temperature and CMB temperature decoupling in some regions around the miniquasar; this effect has been recently point out by Chuzhoy, Alvarez & Shapiro (2006). For recent papers that discuss X-ray heating, see Chen & Miralda-Escude (2006) and Pritchard & Furlanetto (2006).

Collisional decoupling of $T_{\rm spin}$ from $T_{\rm CMB}$ is caused by very energetic electrons released by the effect of the X-ray miniquasar radiation on the IGM. Shull & van Steenberg (1985) have estimated that more than a tenth of the energy of the incident photons is absorbed by the surrounding medium as heating (this fraction increases rapidly with the ionized fraction). The increase in the temperature is observable at radio frequencies in terms of the differential brightness temperature, $\delta T_{\rm b}$, which measures the 21-cm intensity relative to the CMB. A similar fraction of the absorbed energy also goes into collisional excitation, where this fraction decreases rapidly with the ionized fraction. These two processes, heating and excitation decouple the spin temperature from the CMB temperature and render the IGM observable through its 21-cm emission.

Recently, Kuhlen & Madau (2005) and Kuhlen, Madau & Montgomery (2006) have performed a detailed numerical study of the influence of 150 $\mathrm{M}_\odot$ IMBH on its surroundings and calculated the gas, spin and brightness temperatures. They have shown that heating by 150 $\mathrm{M}_\odot$ IMBH at $z = 17.5$ can enhance the 21-cm emission from the warm neutral IGM. The filaments enhance the signal even further and may make the IGM visible in future radio experiments (e.g. the LOFAR-Epoch of Reionization key science project[1]).

In this paper, we adopt a complementary theoretical approach to the numerical one adopted by Kuhlen & Madau (2005). This allows us to explore the influence of power-law radiation fields from a range of black hole masses that are presumed to reside in the centres of primordial miniquasars. Furthermore, the effect of X-ray-induced collisional excitations on the 21-cm spin temperature is included (Chuzhoy et al. 2006) – this effect is not taken into account in the Kuhlen & Madau (2005) work. We test two main classes of X-ray emitting miniquasars, those with UV ionizing radiation and those without. We show that in both cases these miniquasars might play an important role in heating the IGM without necessarily ionizing it completely.

In addition, two simple scenarios for the formation of (mini)quasars as a function of redshift are presented. This is done using the extended Press–Schechter algorithm to predict the number density of forming black holes either with H_2 cooling or with atomic cooling. We also discuss the implications of these scenarios for the mass density of quasars at redshift 6, the SXRB in the energy range 0.5–2 keV (Dijkstra et al. 2004), the number of ionizing photons per baryon and, finally, the optical depth for Thomson scattering of CMB photons.

The paper is organized as follows. Section 2 describes the theoretical methods used here and derives the ionization and kinetic temperature profiles around miniquasars without UV ionizing radiation. Section 3 calculates the spin and brightness temperature around the same quasars. In Section 4 we show the ionization and heating profiles around quasars with UV ionizing radiation. Section 5 presents the two formation scenarios and their implications. The paper concludes with a summary in Section 6.

2 HEATING AND KINETIC TEMPERATURE

The exact shape of the UV and X-ray photon spectral energy distribution around high-redshift miniquasars is uncertain. However, in general it is believed to have two continuum components. The first is through to emanate from the putative accretion disc around a black hole; this component, at least in low-mass black holes, is well described by 'multicolour disc blackbody' (Mitsuda et al. 1984). The hottest blackbody temperature, $T_{\rm max}$, in a Keplerian disc damping material on to a black hole at the Eddington rate is $kT_{\rm max} \approx 1\,\mathrm{keV}\,(M/\mathrm{M}_\odot)^{-1/4}$ (Shakura & Sunyaev 1973), where the hole mass, M, is measured in solar mass units. The characteristic multicolour disc spectrum follows a power law with $L_{\rm E} \propto E^{1/3}$ at $E < kT_{\rm max}$. The second component spectrum is a simple power law with spectral energy distribution proportional to $E^{-\alpha}$ with $\alpha \approx 1$. The precise origin of this power law is uncertain and very likely to be due to non-thermal processes.

To simplify the calculation, we follow Kuhlen & Madau (2005) and consider miniquasars with power-law flux spectra and power-law index of -1. We also assume, at this stage, that the ionizing UV photons produced by the miniquasars are absorbed by the immediate black hole environment. Therefore a lower cut-off of the photon energies is assumed, namely,

$$F(E) = \mathcal{A} E^{-1}\ \mathrm{s}^{-1} \qquad \{200\ \mathrm{eV} \leqslant E \leqslant 100\ \mathrm{keV}\}, \tag{1}$$

where $\mathcal{A}$ is normalized such that the miniquasar luminosity is a tenth of the Eddington luminosity. Miniquasars with UV ionizing photons are considered in a later stage in this paper.

This spectrum translates to a number of photons per unit time per unit area at distance r from the source:

$$\mathcal{N}(E; r) = \mathrm{e}^{-\tau(E;r)} \frac{\mathcal{A}}{4\pi r^2} E^{-1}\ \mathrm{cm}^{-2}\mathrm{s}^{-1}, \tag{2}$$

with

$$\tau(E; r) = \int_0^r n_{\rm H} x_{\rm H\,I} \sigma(E)\, \mathrm{d}r. \tag{3}$$

[1] For more details on the LOFAR radio telescope see http://www.lofar.org.

Here $x_{\rm H\,I}$ is the hydrogen neutral fraction, $n_{\rm H} \approx 1.9 \times 10^{-7}\,{\rm cm}^{-3}\,(1+z)^3$ (Spergel et al. 2006) is the mean number density of hydrogen at a given redshift, and $\sigma_{\rm H}(E) = \sigma_0(E_0/E)^3$ is the bound–free absorption cross-section for hydrogen with $\sigma_0 = 6 \times 10^{-18}\,{\rm cm}^2$ and $E_0 = 13.6\,{\rm eV}$. The second equation is obtained assuming a homogeneous density for the IGM.

The cross-section quoted earlier does not take into account the presence of helium. In order to include the effect of helium, we follow Silk et al. (1972) who modified the cross-section to become

$$\sigma(E) = \sigma_{\rm H}(E) + \frac{n_{\rm He}}{n_{\rm H}}\sigma_{\rm He} = \sigma_1\left(\frac{E_0}{E}\right)^3. \tag{4}$$

A proper treatment of the effect of helium is accounted for by defining σ_1 to be a step function at the two helium ionization energies corresponding to He I and He II. This however includes lengthy calculations and complicates the treatment, and we therefore choose σ_1 to be a smooth function of E, an approximation that will overestimate $\sigma(E)$ for low-energy photons. For the kinds of spectra and energies we consider here, this is a reasonable assumption.

2.1 Ionization

To obtain the optical depth at a given distance, r, from the miniquasar, we calculate the neutral fraction around the miniquasar for a given spectrum and energy range by solving the ionization-recombination equilibrium equation (Zaroubi & Silk 2005):

$$\alpha^{(2)}_{\rm H\,I} n^2_{\rm H}(1 - x_{\rm H\,I})^2 = \Gamma(r)\, n_{\rm H} x_{\rm H\,I}\left(1 + \frac{\sigma_{\rm He}}{\sigma_{\rm H}}\frac{n_{\rm He}}{n_{\rm H}}\right). \tag{5}$$

Here $\Gamma(r)$ is the ionization rate per hydrogen atom at distance r from the source. Since we are interested in the detailed structure of the ionization front, Γ is calculated separately for each value of r using the expression

$$\Gamma(r) = \int_{E_0}^{\infty} \sigma(E)\mathcal{N}(E; r)\left[1 + \frac{E}{E_0}\,\phi(E, x_{\rm e})\right]\frac{{\rm d}E}{E}. \tag{6}$$

The function $\phi(E,\, x_{\rm e})$ is the fraction of the initial photon energy that is used for secondary ionizations by the ejected electrons and $x_{\rm e}$ is the fraction of ionized hydrogen (Shull & van Steenberg 1985; Dijkstra et al. 2004). The $(E/E_0)\,\phi(E,\, x_{\rm e})$ term is introduced to account for the number of ionization introduced by secondary ionization. Furthermore, in equation (5) $\alpha^{(2)}_{\rm H\,I}$ is the recombination cross-section to the second excited atomic level and has the values of $2.6 \times 10^{-13}\ T_4^{-0.85}\,{\rm cm}^3\,{\rm s}^{-1}$, with T_4 being the gas temperature in units of 10^4 K. For this calculation we assume that $T = 10^4$ K. This is of course not very accurate, although it gives a lower limit on the recombination cross-section, $\alpha^{(2)}_{\rm H\,I}$ (in neutral regions atomic cooling prevents the gas from having a higher temperature). Since the region we are going to explore is mostly neutral, an accurate estimation of the recombination cross-section is not necessary.

Fig. 1 shows the solution of equation (5) for miniquasars with masses ranging from $50\,{\rm M}_{\odot}$ up to $2.5 \times 10^4\,{\rm M}_{\odot}$. We assume that the miniquasars emit at a tenth of the Eddington luminosity and that their emitted radiation is confined to $200 \leqslant E \leqslant 10^5$ eV. The lack of ionizing UV photons results in a very small ionized region around the miniquasar centres (X-ray photons are not very efficient in ionization) with an extended transitional region between the ionized and the neutral IGM (Zaroubi & Silk 2005). We also assume that the density of the IGM around the miniquasars is the mean density in the Universe (this could be easily replaced by any spherical density profile). Due to the increase of the mass density at higher redshifts, the ionizing photons are absorbed closer to the quasar. The neutral fraction profile obtained for each profile is used in the following sections to calculate the kinetic, spin and brightness temperatures of the IGM surrounding the miniquasars.

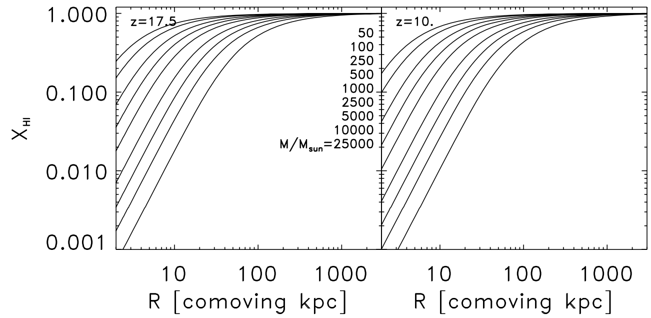

Figure 1. The neutral hydrogen fraction as a function of distance for a range of black hole masses for $z = 17.5$ (left-hand panel) and $z = 10$ (right-hand panel) for miniquasars without ionizing UV radiation, namely, with radiation that spans the energy range of $200 < E < 10^5$ eV.

2.2 Heating

The heating rate per unit volume per unit time that is produced by the photons absorbed by the IGM for a given photon energy at distance r from the source is $\mathcal{H}(r).\mathcal{H}$ is calculated separately for each r using the expression

$$\mathcal{H}(r) = f n_{\rm H} x_{\rm H\,I}(r)\int_{E_0}^{\infty}\sigma(E)\mathcal{N}(E; r)\,{\rm d}E, \tag{7}$$

where f is the fraction of the absorbed photon energy that goes into heating through collisional excitations of the surrounding material (Shull & van Steenberg 1985). The function f is fitted in the Shull & van Steenberg (1985) paper with the following simple fitting formula: $f = C\,[1 - (1 - x^a)^b]$, where $C = 0.9771$, $a = 0.2663$, $b = 1.3163$ and $x = 1 - x_{\rm H\,I}$ is the ionized fraction. This fitting function is valid in the limit of high photon energies, an appropriate assumption for the case at hand. We only modify the fitting formula by imposing a lower limit of 11 per cent for the fraction of energy that goes into heating as the proposed fitting formula does not work well at ionized hydrogen fractions smaller than 10^{-4}. This equation is similar to that obtained by Madau et al. (1997).

In order to determine the temperature of the IGM due to this heating, we adopt the following equation,

$$\frac{3}{2}\frac{n_{\rm H}k_{\rm b}T_{\rm kin}(r)}{\mu} = \mathcal{H}(r)t_{\rm q}. \tag{8}$$

Here, $T_{\rm kin}$ is the gas temperature due to heating by collisional processes, $k_{\rm b}$ is the Boltzmann constant, μ is the mean molecular weight and $t_{\rm q}$ is the miniquasar lifetime. This equation assumes that the heating rate due to the absorption of X-ray photons during the miniquasar lifetime is constant. Given the miniquasar lifetime relative to the age of the Universe at the redshifts we are interested in, cooling due to the expansion of the Universe can be safely neglected. Notice that in the highly ionized regions, although we ignore it, Compton cooling off CMB photons for long-living miniquasars and high redshifts should be included.

Fig. 2 shows the kinetic temperature as a function of radius for the same black hole masses considered in Fig. 1. The heating of the IGM is clearly very extended and ranges from about a quarter of a comoving Mpc for a black hole with $50\,{\rm M}_{\odot}$ up to more than 3 comoving Mpc for black holes with masses $\gtrsim 10^4\,{\rm M}_{\odot}$. Since the mass

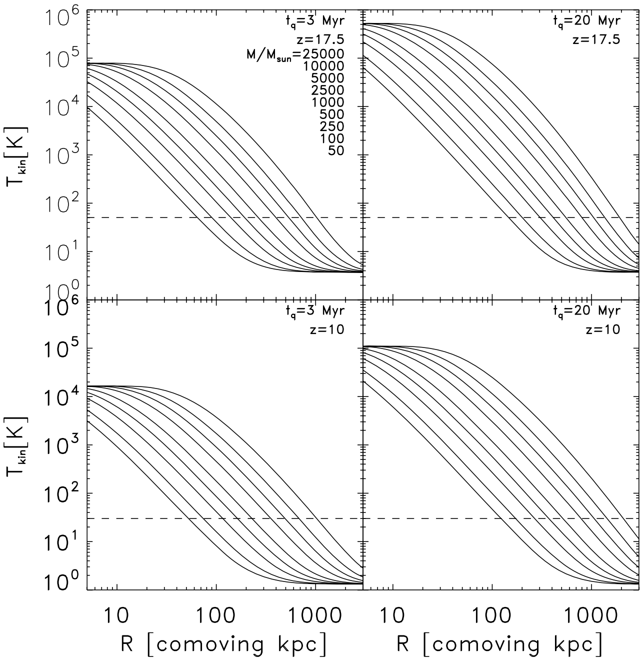

Figure 2. The kinetic temperature of the gas for a range of black hole masses. The redshift and quasar lifetime ($t_{\rm q}$) are specified on each panel. The dashed line indicates the CMB temperature at the corresponding redshift.

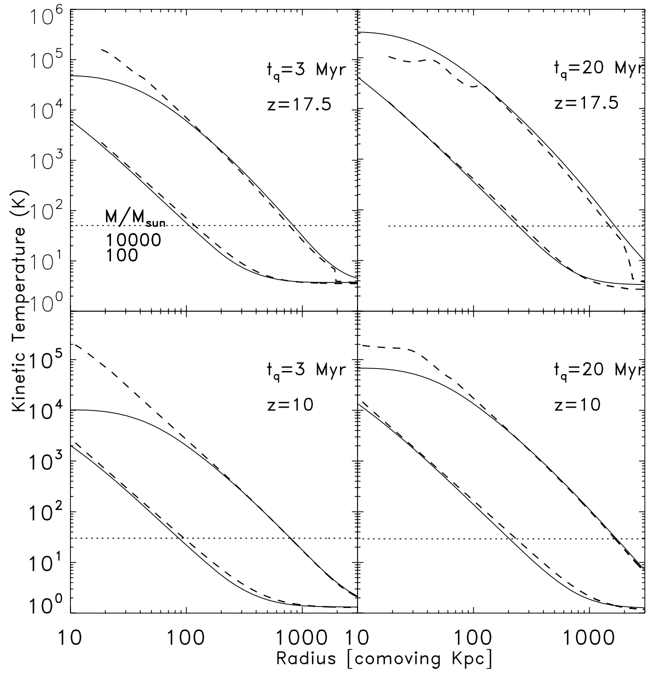

Figure 3. A comparison between the model adopted in this study and the results from a spherically symmetric radiative transfer code (Thomas & Zaroubi, in preparation) applied to two of the IMBH masses, 100 and 10 000 $M_\odot$ with the same radiation power spectrum. The analytical calculation is represented by the solid line and that obtained from the radiative transfer code is represented by the dashed line. The dotted line indicates the CMB temperature at the corresponding redshift.

density in the Universe increases towards higher z as $(1+z)^3$, the neutral fraction around the miniquasar is larger, hence, the heating is more effective at higher redshifts. The figure also shows that, as expected, the heating is larger for a quasar with a longer lifetime. Note, that at redshift 10 other effects (e.g. Lyman α pumping, metal cooling lines) might play a more important role than heating by miniquasars. However, the purpose of presenting the $z=10$ figures is to show the redshift trend of change due to miniquasars.

2.3 Comparison with a spherically symmetric full radiative transfer code

In order to test our analytical approach we compare our results with those obtained by running a non-equilibrium spherically symmetric radiative transfer code that is applied to the same problem. Details of the code are described by Thomas & Zaroubi (in preparation) but here we give a brief description. The radiative transfer code evolves non-equilibrium equations for H I, H II, He I, He II, He III, e and the electron temperature $T_{\rm e}$. The equations take into account collisional and photoionization, recombination, collisional excitation cooling, recombination cooling, free–free cooling, Hubble cooling, Compton heating and Compton cooling. The comparison between the analytical and the numerical results is performed for eight cases. The eight cases constitute all combinations of two black hole masses (100 and 10 000), two redshifts (10 and 17.5) and two miniquasar lifetimes (3 and 20 Myr). The comparison is shown in Fig. 3 where the kinetic temperature of the gas obtained from the simple analytical calculation is represented by the solid line and that obtained from the radiative transfer code is represented by the dashed line. Except at the centre where the neutral fraction adopted profile differs in the two cases, the agreement between the two approaches is very good. The main reason for the departure in the centre is that the equilibrium solution assumes that the neutral fraction profile shown in Fig. 1 is attained within the quasar lifetime; this assumption is simply incorrect for high-energy photons where the bound–free time-scales exceeds that (for a recipe to mitigate this effect see Thomas & Zaroubi, in preparation). To summarize, given the many processes included in the radiative transfer code, this agreement is satisfactory.

Another comparison one can make is with the gas temperatures obtained by Kuhlen & Madau (2005) shown in the upper right-hand panel of fig. 7 in their paper. Visual inspection of the results of our approach when applied to a 150 $M_\odot$ IMBH with the same spectrum shows good agreement. Both of these comparisons give us confidence in the validity of the simplistic theoretical approach adopted in this paper.

3 21-CM SPIN AND BRIGHTNESS TEMPERATURES

3.1 The spin temperature

In his seminal paper, Field (1958; see also Kuhlen et al. 2006) used the quasi-static approximation to calculate the spin temperature, $T_{\rm spin}$, as a weighted average of the CMB temperature, the gas kinetic temperature and the 'light' temperature related to the existence of ambient Lyman α photons (Wouthuysen 1952; Field 1958). The spin temperature is given by

$$T_{\rm spin} = \frac{T_* + T_{\rm CMB} + y_{\rm kin} T_{\rm kin} + y_\alpha T_{\rm kin}}{1 + y_{\rm kin} + y_\alpha}, \tag{9}$$

where $T_{\rm CMB}$ is the CMB temperature and $y_{\rm kin}$ and y_α are the kinetic and Lyman α coupling terms, respectively.

The kinetic coupling term is due to the increase in the kinetic temperature due to X-ray heating.

$$y_{\rm kin} = \frac{T_*}{A_{10}T_{\rm kin}}(C_{\rm H} + C_{\rm e} + C_{\rm p}). \quad (10)$$

Here $A_{10} = 2.85 \times 10^{-15}\ {\rm s}^{-1}$ (Wild 1952) is the Einstein spontaneous emission rate coefficient. $C_{\rm H}$, $C_{\rm e}$ and $C_{\rm p}$ are the de-excitation rates due to neutral hydrogen, electrons and protons, respectively. These rates have been calculated by several authors (Field 1958; Smith 1966; Allison & Dalgarno 1969; Zygelman 2005). In this paper we use the fitting formulae used in Kuhlen et al. (2006) which we repeat here for completeness, the rate due to neutral hydrogen $C_{\rm H} = 3.1 \times 10^{-11} n_{\rm H} T_{\rm kin}^{0.357}\ \exp\ (-32/T_{\rm kin})\ ({\rm s}^{-1})$; the rate due to electrons is $C_{\rm e} = n_{\rm e}\gamma_{\rm e}$ where $\log(\gamma_{\rm e}/1\ {\rm cm}^3\ {\rm s}^{-1}) = -9.607 + 0.5 \log T_{\rm kin} \exp[-(\log\ T_{\rm kin})^{4.5}/1800]$; and the rate due to protons is $C_{\rm p} = 3.2\, n_{\rm p}\,\kappa$, where $\kappa = C_{\rm H}/n_{\rm H}$ is the effective single-atom rate coefficient. And $n_{\rm H}$, $n_{\rm e}$ and $n_{\rm p}$ are the hydrogen, electron and proton number densities in the unit of ${\rm cm}^{-3}$, respectively, and $T_{\rm kin}$ is measured in K.

The Lyman α coupling term is also due to collisional excitation. Previously, studies that have considered X-ray heating have ignored this effect. Recently however, Chuzhoy et al. (2006) have pointed out that this contribution is very important and even dominates the spin temperature value in a certain temperature range. In order to account for this term one should calculate the intensity of the Lyman α photons due to collisional excitations, J_0. This is given by the following equation:

$$J_0(r) = \frac{\phi_\alpha\, c}{4\pi H(z)\nu_\alpha} n_{\rm H} x_{\rm H\,I}(r) \int_{E_0}^{\infty} \sigma(E)\mathcal{N}(E;r)\,{\rm d}E. \quad (11)$$

This equation is similar to equation (7) except that instead of the fraction of the absorbed energy that goes to heat, *f*, one should use the fraction of the absorbed energy that goes into kinetic excitation of Lyman α. The fraction, ϕ_α, is also parametrized by Shull & van Steenberg (1985) and is given by $\phi_\alpha \approx 0.48\ (1 - x^{0.27})^{1.52}$ (where $x = 1 - x_{\rm H\,I}$). In the equation above, c is the speed of light and ν_α is the Lyman α transition frequency. The Hubble constant as a function of redshift, $H(z)$, is calculated assuming $\Omega_{\rm m} = 0.24$ and $\Omega_\Lambda = 0.76$.

The y_α coupling term is (Field 1958)

$$y_\alpha = \frac{16\pi^2 T_* e^2 f_{12} J_0}{27 A_{10} T_{\rm kin} m_{\rm e} c}. \quad (12)$$

Here, $f_{12} = 0.416$ is the oscillator strength of the Lyman α transition, A_{10} is the Einstein spontaneous emission coefficient of the 21-cm transition and e and $m_{\rm e}$ are the electron charge and mass, respectively.

Fig. 4 shows the spin temperature of the gas for a range of black hole masses. The redshift and quasar lifetime ($t_{\rm q}$) are specified on each panel. The figure clearly shows that as the distance from the miniquasar increases, the temperature drops to the $T_{\rm CMB}$ level. The distance at which the temperature reaches the $T_{\rm CMB}$ asymptotic value depends on the black hole mass. For the more massive black holes, this distance can exceed a couple of comoving Mpc.

The figure also shows that the maximum spin temperature is almost independent of the quasar mass – a detailed inspection of the figure shows a slight change in the maximum of $T_{\rm spin}$ as a function of mass. This effect is due to the fact that the dominant coupling parameter in equation (9) around the maximum $T_{\rm spin}$ is y_α (by at least an order of magnitude) and is of the order of 0.01. Under such conditions equation (9) reduces to $T_{\rm spin} \approx y_\alpha T_{\rm kin}$, namely, $T_{\rm spin} \propto J_0$. J_0 in regions where $x_{\rm H\,I} \ll 1$ is independent of quasar mass as implied by the left-hand side of equation (5). Physically, this means that when the medium is already ionized no additional heating of the IGM due to bound–free absorption is possible, no matter how much radiation comes out of the quasar.

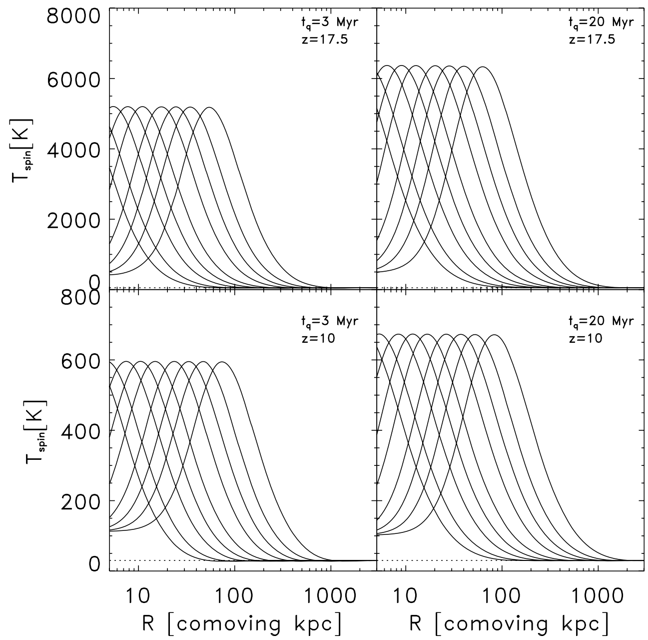

Figure 4. The spin temperature of the gas for a range of black hole masses. The redshift and quasar lifetime ($t_{\rm q}$) are specified on each panel. The dotted line indicates the CMB temperature at the corresponding redshift. Note the different y-axis range between the $z = 17.5$ and 10 panels.

3.2 The brightness temperature

In radio astronomy, where the Rayleigh–Jeans law is usually applicable, the radiation intensity, $I(\nu)$ is expressed in terms of the brightness temperature, so that

$$I(\nu) = \frac{2\nu^2}{c^2} k_{\rm b} T_{\rm b}, \quad (13)$$

where ν is the radiation frequency, c is the speed of light and k is Boltzmann's constant (Rybicki & Lightman 1979). This in turn can only be detected differentially as a deviation from $T_{\rm CMB}$, the CMB temperature. The predicted differential brightness temperature deviation from the CMB radiation, at the mean density, is given by (Field 1958, 1959; Ciardi & Madau 2003)

$$\delta T_{\rm b} = (20\ {\rm mK})\,(1+\delta)\left(\frac{x_{\rm H\,I}}{h}\right)\left(1 - \frac{T_{\rm CMB}}{T_{\rm spin}}\right) \times \left(\frac{\Omega_{\rm b}h^2}{0.0223}\right)\left[\left(\frac{1+z}{10}\right)\left(\frac{0.24}{\Omega_{\rm m}}\right)\right]^{1/2}, \quad (14)$$

where h is the Hubble constant in units of $100\,{\rm km\,s^{-1}\,Mpc^{-1}}$, δ is the mass density contrast, and $\Omega_{\rm m}$ and $\Omega_{\rm b}$ are the mass and baryon densities in units of the critical density. We also adopt a standard model universe with a flat geometry, $\Omega_{\rm b}\,h^2 = 0.022$, $\Omega_{\rm m} = 0.24$ and $\Omega_\Lambda = 0.76$ (Spergel et al. 2006).

Fig. 5 shows the brightness temperature for the same IMBH mass explored in Fig. 2. The curves show that the radius at which the differential brightness temperature is detectable increases with the black hole mass and the miniquasar lifetime (left-hand versus right-hand panels). The maximum amplitude, however, does not depend on the black hole mass and depends only weakly on the miniquasar

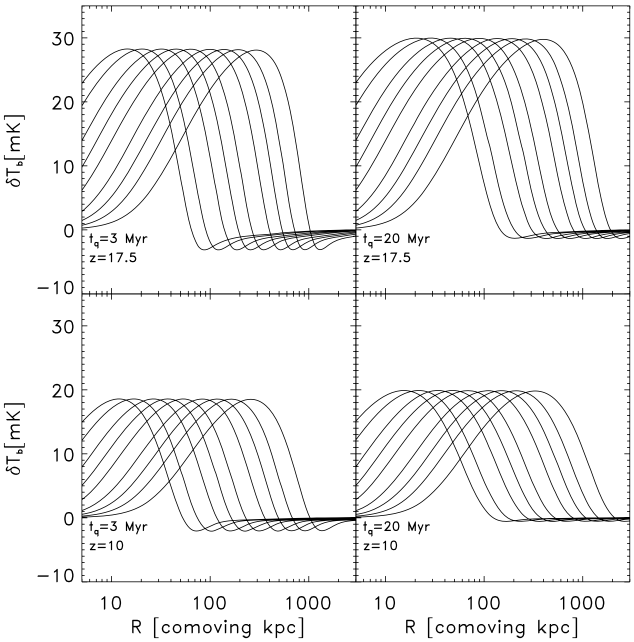

Figure 5. The brightness temperature for the same cases shown in Fig. 4.

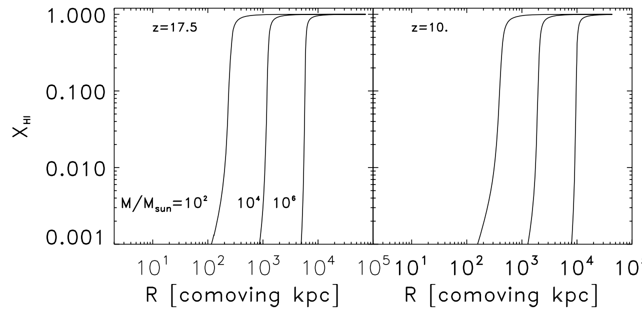

Figure 6. The neutral hydrogen fraction as a function of distance for three black hole masses (100, 10^4 and 10^6 $M_\odot$) for $z = 17.5$ (left-hand panel) and $z = 10$ (right-hand panel) for miniquasars with UV ionization energy, that is, emitted radiation that spans the energy range 10.4 to $\sim 10^4$ eV.

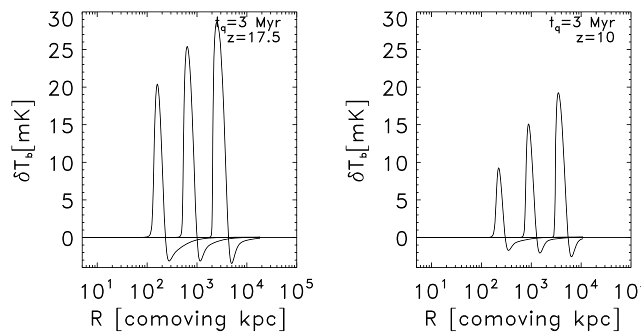

Figure 7. The differential brightness temperature for three miniquasars with black hole masses 100, 10^4 and 10^6 $M_\odot$ and ionizing UV and X-ray photons (i.e. energy range of $10.4 < E < 10^4$ eV). The quasar lifetime here is 3 Myr.

lifetime. This is because at the centre, $T_{\rm spin} \gg T_{\rm CMB}$. Hence $\delta T_{\rm b}$ is at its maximum value which, at the mean density of the Universe, only depends on the redshift and cosmological parameters.

4 MINIQUASARS WITH IONIZING UV RADIATION

We consider the signature of (mini)quasars with UV radiation that ionizes the IGM. The different options for quasar spectral energy distribution have been discussed earlier. Here we follow Madau et al. 2004 and assume that the radiation flux spectrum is the same as in equation (1), except that the energy spans the range of 10.4–100 keV. Of course in this case the quasar will ionize its immediate surroundings and heat up a more extended region of the IGM, a realistic spectrum will probably be between this case and the previous case of truncated power law (see Section 5 for a more complex energy spectrum). Here we test three black hole masses of 100, 10^4 and 10^6 $M_\odot$ at $z = 10$ and 17.5 with lifetimes of 3 Myr. The 10^6 $M_\odot$ mass objects could be considered as progenitors of the SDSS $z \approx 6$ quasars. The H I neutral fraction as a function of distance from the quasar is shown in Fig. 6 for the three black hole masses at $z = 17.5$ (left-hand panel) and $z = 10$ (right-hand panel).

If one assumes that the IGM is not heated relative to the CMB, then the quasar will heat its environment but appears as an emission shell around the quasar in the 21-cm brightness temperature maps. Fig. 7 shows the differential brightness temperature around the same three black hole masses shown in Fig. 6. The clear difference in the brightness temperature between this figure and Fig. 5 is due to the size of the ionized region around the (mini)quasar.

5 QUASAR FORMATION AND EVOLUTION

5.1 Quasar evolution with redshift

In this section we propose two very simple scenarios for the production and evolution of quasars at high redshift and explore the implications for IGM heating, ionization and the observed X-ray background (XRB) (Moretti et al. 2003; Sołtan 2003). We evaluate the initial mass density of black holes as a function of redshift, without mass accretion, with the following formation scenarios: (i) black holes as end products of stars that have formed through molecular hydrogen cooling, that is, stars formed in haloes with virial temperatures smaller than 10^4 K. (ii) black holes that have been produced directly through the collapse of massive low angular momentum haloes. In both cases, we use the Press–Schechter (Press & Schechter 1974) formalism with the Sheth & Tormen (1999) mass function to infer the number density of haloes with a given mass as a function of redshift.

The mass density of black holes for the first scenario is estimated simply by calculating the number density of the most massive haloes with molecular hydrogen cooling. These are haloes in the range of $0.1M_{T_4} \leqslant M \leqslant M_{T_4}$, where M_{T_4} is the mass of a halo with virial temperature 10^4 K. This is a rough approximation for haloes that have efficient self-shielding for H_2 disassociation and can form pop III stars through molecular hydrogen cooling (Haiman, Rees & Loeb 1997a,b). We henceforth refer to this scenario as the intermediate mass black hole (IMBH) scenario. To estimate the comoving mass density of the forming black holes as a function of redshift, we assume that at the centre of these massive haloes, the star ends its life as a 100 $M_\odot$ $\times$ $(M_{\rm halo}/M_{T_4})$ black hole. The mass density of the forming black holes as a function of redshift is presented by the thick solid line shown in the upper panel of Fig. 8.

For the second scenario, we estimate the number of haloes with atomic hydrogen cooling, namely haloes with virial temperature $T_{\rm virial} \geqslant 10^4$ K. In order to estimate the comoving mass density of black holes per comoving Mpc^3 produced by this scenario, we assume that only 1 per cent of the haloes in this mass range have a

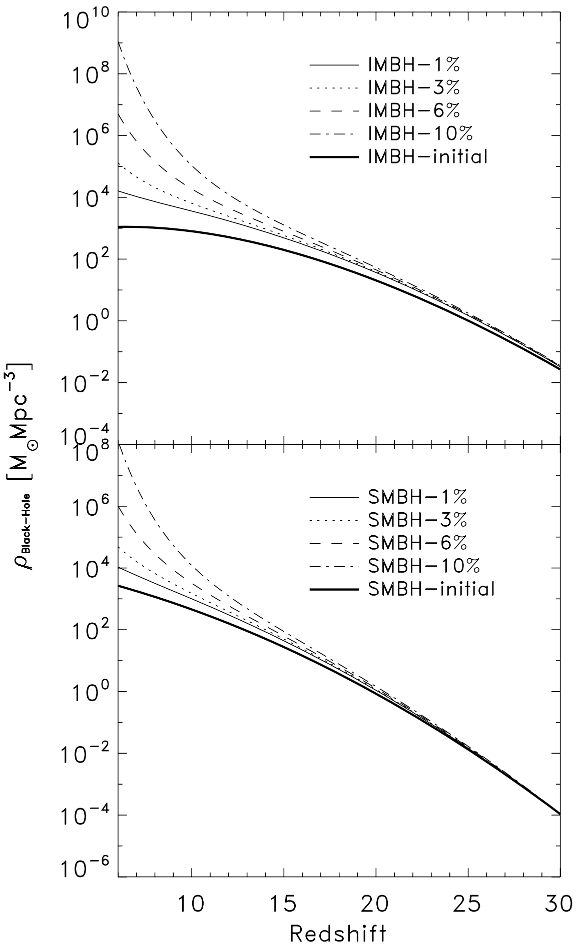

Figure 8. Initial and evolving comoving black hole mass density as a function of redshift. The solid thick line shows the mass density of forming black holes as a function of redshift. The other four lines show the total comoving mass density for four values of $f_{\rm duty}$. The IMBH results are shown in the upper panel and those for the SMBH case are shown in the lower panel.

low enough spin parameter to allow a direct collapse of the halo to form a massive black hole. The distribution of the spin parameter of haloes is quite flat at the low end of the possible spin parameter range (Steinmetz & Bartelmann 1995), and therefore, the choice of 1 per cent is rather conservative. In these haloes, we take the mass that ends up in black holes as $10^{-3} \times (\Omega_{\rm b}/\Omega_{\rm m})\, M_{\rm halo}$, where the 10^{-3} reflects the Magorian relation between the halo mass and black hole mass, and $\Omega_{\rm b}/\Omega_{\rm m}$ gives the baryon ratio. The comoving mass density of black holes produced in this type of scenario is presented by the solid thick line shown in the lower panel of Fig. 8. We refer to this model as the SMBH scenario.

To calculate the accumulated comoving black hole mass density at any redshift, we assume that the black hole is accreting at the Eddington rate with a given radiative efficiency, $\epsilon_{\rm rad}$. The radiative efficiency is fixed in this paper to be 10 per cent. The cumulative comoving mass density is then given by the following equation:

$$\tilde{\rho}(z) = \int_z^{35} {\rm d}z' \rho(z') \times \exp\left\{ f_{\rm duty} \left[\frac{t(z) - t(z')}{t_{\rm E}}\right] \frac{1-\epsilon_{\rm rad}}{\epsilon_{\rm rad}} \right\} \left({\rm M}_\odot\ {\rm Mpc}^{-3}\right), \quad (15)$$

where $f_{\rm duty}$ is the duty cycle, which ranges from 1 to 10 per cent, $t(z)$ is the age of the universe at redshift z and $t_{\rm E} \equiv 0.41$ Gyr is the Eddington time-scale.

The thin lines shown in Fig. 8 show the comoving black hole mass density as a function of redshift for several $f_{\rm duty}$ values. The calculation is done for both IMBH and SMBH scenarios. The case with $f_{\rm duty} = 10$ per cent produces a black hole density relative to the critical density of $\Omega_{\rm black\,hole}(z = 6) \sim 10^{-3}$ and 10^{-4} for the IMBH and SMBH scenarios, respectively. These values are too high to be compatible with the inferred black hole density at redshift 6. The other extreme case with $f_{\rm duty} = 1$ per cent produces $\Omega_{\rm black\,hole}(z = 6) \sim 10^{-8}$ for both scenarios, which is too low. Therefore, in the following subsections, we will focus on the results obtained from the cases with $f_{\rm duty} = 3$ and 6 per cent.

Recently, Begelman, Volonteri & Rees (2006) have estimated build-up of the black hole mass density at the high-redshift Universe that form via the 'bars within bars' mechanism. This mechanism allows for the SMBHs to form directly in the nuclei of protogalaxies, without the need for 'seed' black holes left over from early star formation. In their paper, Begelman et al. (2006) showed black hole density as a function of redshift for two duty duty cycles, $f_{\rm duty} = 0.1$ and 0.5. Unlike in our simple model, their model gives a rapid increase in the mass density of black holes until $z \approx 18$ after which the black hole density evolves relatively slowly (roughly as $\log \rho_{\rm black\,hole} = {\rm constant} + 0.086z - 0.009z^2$, which is obtained from a cubic spline fit to their fig. 2). To summarize, according to Begeleman et al. the black hole density attains relatively high values early on but evolves slowly afterwards, whereas our model the initial density is low but the mass evolution is more rapid.

Whichever the actual scenario of the evolution of black holes mass density in the Universe, it is clear that the mass densities obtained at high redshift contribute significantly to heating the IGM and decouple the spin temperature from the CMB temperature (see Figs 5 and 7). In the next section, we explore which of the scenarios we explore is consistent with the currently available observational constraints.

5.2 The soft X-ray background constraint

Recently, Dijkstra et al. (2004) and Salvaterra et al. (2005) have shown that it is very unlikely that miniquasars have ionized the Universe without violating the observed SXRB luminosity in the energy range 0.5–2 keV (Moretti et al. 2003). In both cases the authors have assumed a specific black hole mass history – instantaneous in the case of Dijkstra et al. and more gradual in the case of Salvaterra et al. (2005). Our aim here is to check whether the specific black hole evolution histories proposed in the current study violate this observational constraint, regardless of whether they ionize the Universe or not.

It will be shown that our adopted quasar duty cycle, limited from above by the Soltan et al. (2003) constraint, yields a diffuse X-ray flux that is consistent with the SXRB constraint. We assume a mean reionization history of the Universe according to which the IGM underwent a sudden reionization at redshift 6. This assumption is insensitive to our computed SXRB flux, and is conservative, in that it provides an upper limit on the ionizing flux from (mini)quasars. The SXRB is calculated for various quasar spectrum templates. The purpose here is twofold. First, to exclude from our models those cases that violate the SXRB constraints. Secondly, to explore the influence of various spectral dependences on the SXRB.

The first template is the one we used for the quasars that have no UV radiation,

$$F(E) = \mathcal{A}\, E^{-\alpha} \quad 200\ \text{eV} < E < 100\ \text{keV}, \tag{16}$$

where the calculation is made for a range of power-law indices, $\alpha = 2$–0. This represents the case in which all the ionizing radiation is absorbed in the immediate vicinity of the quasar. The case we explored previously for the heating and ionization fronts was specifically for $\alpha = 1$.

The second template, which we have also used before, represents the case in which all the UV radiation escapes the quasar's immediate surroundings into the IGM. The template used here is

$$F(E) = \mathcal{A}\, E^{-\alpha} \quad 10.4\ \text{eV} < E < 100\ \text{keV}, \tag{17}$$

where α spans the same range as before.

The third case we explore is the one with the template introduced by Sazonov, Ostriker & Sunyaev (2004) and has the form

$$F(E) = \begin{cases} \mathcal{A}\, E^{-1.7} & \text{if } 10.4\ \text{eV} < E < 1\ \text{keV}, \\ \mathcal{A}\, E^{-\alpha} & \text{if } 1 < E < 100\ \text{keV}, \\ \mathcal{A}\, E^{-1.6} & \text{if } E > 100\ \text{keV}. \end{cases}$$

Notice here that we keep the power-law index of the middle range, α, as the varying parameter. The reason is that quasars in the redshift range 6–10 with a Sazonov et al. type spectrum contribute to the observed SXRB mainly in the energy range 0.5–2 keV.

To proceed, we normalize the above equation with respect to the product of the Eddington luminosity and the radiation efficiency, $\epsilon_{\rm rad}$. This should be done at a given distance, *r*, from the quasar which we choose arbitrarily to be 1 Mpc.

A quasar of mass *M* shines at $\epsilon_{\rm rad}$ times the Eddington luminosity, namely

$$L_{\rm Edd}(M) = 1.38 \times 10^{38} \left(\frac{M}{\rm M_{\odot}}\right)\ (\text{erg s}^{-1}). \tag{18}$$

Therefore $\mathcal{A}$ is given by

$$\mathcal{A}(M) = \frac{\epsilon_{\rm rad}\ L_{\rm Edd}(M)}{\int_{E_{\rm range}} E^{-\alpha}\ {\rm d}E \times 4\pi r^2}\ (\text{erg}^{\alpha}\ \text{s}^{-1}\ \text{cm}^{-2}), \tag{19}$$

where $E_{\rm range} = 10.4$–100 keV.

In order to calculate the SXRB, we follow Dijkstra et al. (2004). The contribution of the SXRB observed in the range $0.5 < E < 2$ keV, given by

$$\text{SXRB} = \left(\frac{\pi}{180}\right)^2 \int_6^{35} {\rm d}z\, {\rm d}_A(z)^2 \frac{\mathcal{A}(\tilde{\rho}(z))}{\left[{\rm d_L}(z)\ \text{Mpc}^{-1}\right]^2} \times \int_{0.5(1+z)}^{2(1+z)} E^{-\alpha}\, {\rm e}^{-\tau(E;z)}\, {\rm d}E\ (\text{erg s}^{-1}\ \text{cm}^{-2}\ \text{deg}^{-2}). \tag{20}$$

In the above equation, $\tau(E;z)$ represents the optical depth,

$$\tau(E; z_{\rm Q}) = \frac{c}{H_{\rm o}\sqrt{\Omega_{\rm m}}} \int_6^{z_{\rm q}} \frac{{\rm d}z}{(1+z)^{5/2}} \times [n_{\rm H\,I}(z)\sigma_{\rm H\,I}(E') + n_{\rm He\,I}(z)\sigma_{\rm He\,I}(E')], \tag{21}$$

where $E' = E(1+z)/(1+z_{\rm Q})$, $z_{\rm Q}$ is the quasar formation redshift, $n_{\rm H\,I}(z) = n_{\rm H\,I}(0)(1+z)^3$ and $n_{\rm He\,I}(z) = n_{\rm He\,I}(0)(1+z)^3$ are the physical density of hydrogen and helium with $n_{\rm H\,I}(0) = 1.9 \times 10^{-7}\ \text{cm}^{-3}$ and $n_{\rm He\,I}(0) = 1.5 \times 10^{-8}\ \text{cm}^{-3}$. The luminosity distance, ${\rm d_L}(z)$, to the black hole is calculated from the fitting formula given by Pen (1999) and ${\rm d}_A$ is the angular diameter distance,

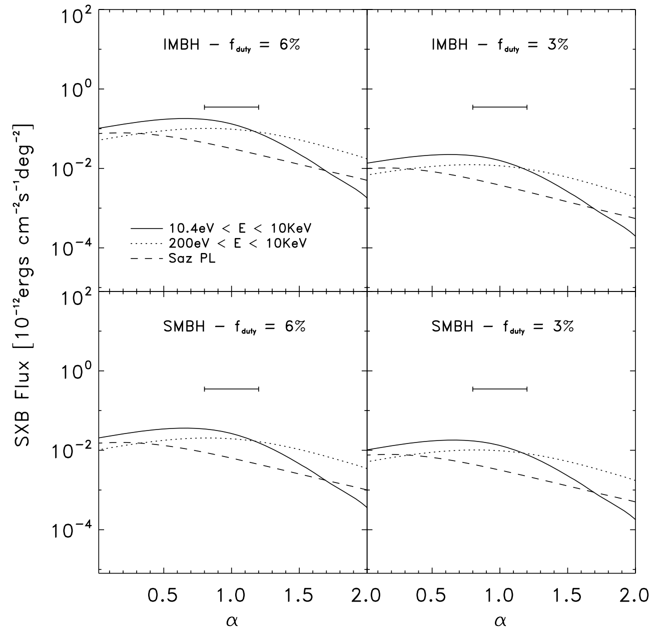

Figure 9. Soft X-ray background for various spectra. The four panels show the SXRB level expected from the IMBH (upper panels) and SMBH (lower panels) scenarios with $f_{\rm duty} = 6$ per cent (right-hand panels) and 3 per cent. Each panel shows the SXRB obtained assuming the three templates: power-law quasars with ionization by UV radiation (solid lines) and without UV radiation (dotted lines) and quasars with the Sazonov et al. (2004) template (dashed lines). The short horizontal line in the middle of each panel marks the observational constraint of Moretti et al. (2003).

$${\rm d}_A(z) = \frac{{\rm d_L}(z)}{(1+z)^2}. \tag{22}$$

The division by ${\rm d_L^2}$ accounts for the dimming of the quasar, whereas the multiplication by $(\pi/180)^2{\rm d}_A^2$ calculates the flux received in a 1-deg^2 field of view. Moreover, the normalization factor is now made with respect to the mass density of black holes, and hence it carries an extra Mpc^{-3} in our units.

Fig. 9 shows the expected SXRB as a function of α for the IMBH and SMBH scenarios in the $f_{\rm duty} = 3$ and 6 per cent cases. The short horizontal line at the middle of each of the panels marks the observational SXRB constraint. This shows that none of these models violate the observational constraint. The 10 per cent case, which is not shown here, violates the observed constraints for almost all the α range.

5.3 The number of ionizing photons per baryon

We now calculate the number of ionizing photons per baryon emitted in the IMBH and SMBH models for the $f_{\rm duty} = 6$ and 3 per cent models. The purpose of this calculation is to show that these models will not be able to ionize the Universe, except in the extreme case in which the escape fraction of the ionizing UV photons is unity and no recombinations take place. To estimate the number of ionizing photons, one should integrate the number of emitted photons per unit energy over the energy spectrum of the quasars. The factor $(1 - {\rm e}^{-\tau})$ accounts for the absorbed fraction of photons. It also involves an integral over the active lifetime of the quasars down to redshift 6. These integrations have the following form:

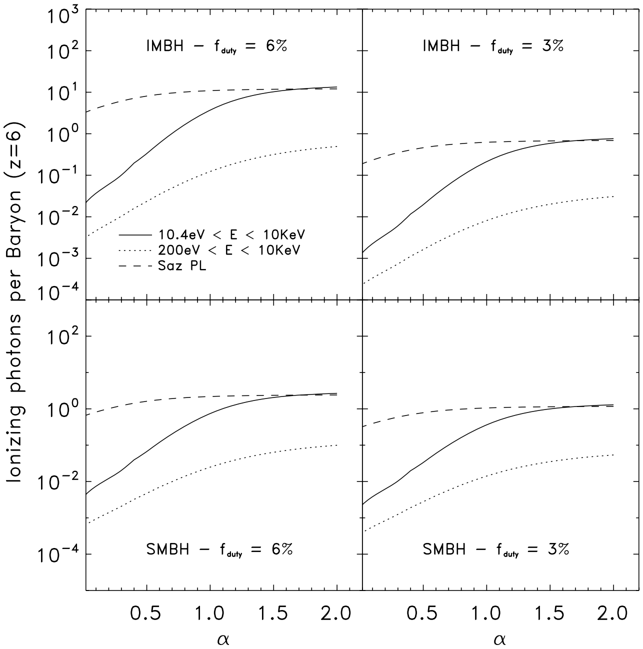

Figure 10. Number of ionizing photons per baryon for different spectra. The upper two panels show results for the IMBH scenario with the left- and right-hand panels assuming $f_{\rm duty} = 6$ per cent and 3 per cent, respectively. The lower two panels show results for the SMBH scenario with the left- and right-hand panels assuming $f_{\rm duty}$ of 6 and 3 per cent. The three models explored are as in the previous figure.

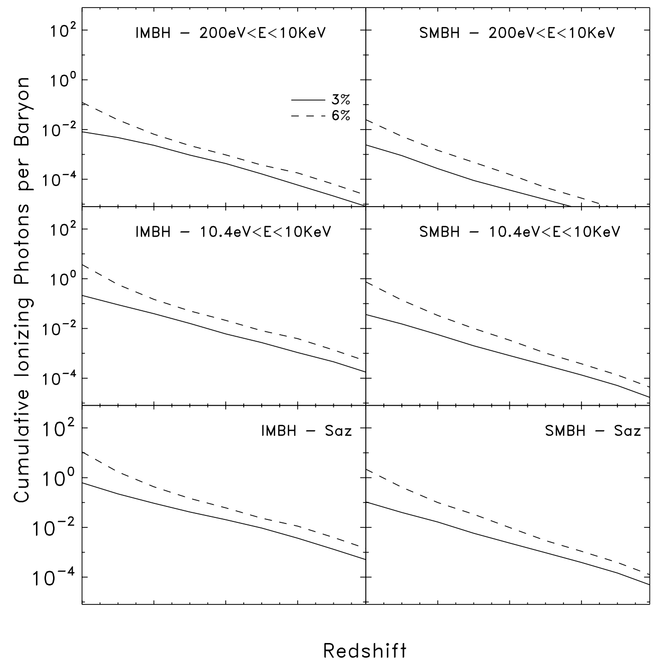

Figure 11. The number of ionizing photons per baryon as a function of redshift. The three left-hand panels refer to the IMBH scenario with each of the three showing the number of ionizing photons per baryon for a different spectral template. The three right-hand panels show the same for the SMBH scenario. These figures assume a power-law index α of 1.

$$N_{\rm photons} = 4\pi \int_{6<z<35} {\rm d}z\ \mathcal{A}(\tilde{\rho}(z))\ \frac{{\rm d}t}{{\rm d}z}\ f_{\rm duty} \times \int_{E_{\rm range}} E^{-\alpha} \left[1 - {\rm e}^{-\tau(E;z)}\right] \frac{{\rm d}E}{E}\ ({\rm Mpc}^{-3}), \tag{23}$$

where dt/dz is given by

$$\frac{{\rm d}t}{{\rm d}z} = \frac{1}{H_{\rm o}\,(1+z)\sqrt{(1+z)^2(1+\Omega_{\rm m}z) - z(2+z)\Omega_\Lambda}}\ ({\rm s}). \tag{24}$$

Again, the mass density parameter $\Omega_{\rm m} = 0.27$ and the vacuum energy density parameter $\Omega_\Lambda = 0.73$. Fig. 10 shows the number of photons per baryon as a function of the energy spectrum power-law index, α. Here we note a number of features. First, the maximum number of ionizing photons per baryon is roughly 10. This number is achieved in the IMBH scenario with $f_{\rm duty} = 6$ per cent for the spectral templates of both Sazonov et al. (dashed line) and the power-law spectrum with ionizing UV radiation (solid line). Despite obtaining such a high number of ionizing photons per baryon, one should note that these two cases assume that all the quasar ionizing photons escape its immediate surroundings. Not surprisingly, the power-law model without ionizing photons does not produce too many ionizations (dotted line). Note also that the number of ionizing photons per baryon produced by the Sazonov et al. model does not vary much with α. This is simply because the power-law index we vary in this model is in the X-ray energy range.

Fig. 11 shows the evolution of the number of ionizing photons per baryon with redshift. The calculation shown here assumes $\alpha = 1$ for all three templates. The three left-hand panels show results for the IMBH scenario, where each of the spectral scenarios is shown in a different panel. The right-hand panels show the same for the SMBH case. As expected, most of the ionizing photons are produced towards the low-redshift range. The Sazonov et al. model produces the largest number of ionizing photons due to its steepness in the low-energy range (power-law index of -1.7). Note, that the $f_{\rm duty} = 6$ per cent case produces about 10 photons per baryon at $z = 6$ normally thought to be enough to ionize the Universe and the same time does not violate the SXRB constraint. However, this model does not reproduce the Thomson τ constraint (see below).

Assuming that these curves give the actual ionization history, one can easily calculate the optical depth for Thomson scattering of CMB photons, $\tau_{\rm CMB}$. This of course is not a self-consistent calculation since in order to obtain the number of ionizing photons as a function of redshift, one has to assume an ionization history. This exercise is still of interest as it gives an upper limit for the influence of quasars on $\tau_{\rm CMB}$. To calculate $\tau_{\rm CMB}$, we assume that the electron density, $n_{\rm e} = n_{\rm H\,I}\, x_{\rm e}$ and $x_{\rm e}$ is given by one-tenth of the number of ionizing photons per baryon that appears in Fig. 11 with an upper limit of unity. The $\tau_{\rm CMB}$ found here for the IMBH model with $f_{\rm duty} = 6$ per cent is about 0.03 which is only one-third of the *WMAP*3 observed value (Page et al. 2006).

5.4 The predicted constraints from the Begelman et al. (2006) model

As an aside, we calculate the SXRB, number of ionizing photons per baryons and the Thomson scattering optical depth for the Begelman et al. (2006) model. Here we choose the case of $f_{\rm duty} = 0.1$ and a rigid disc model, namely, the dotted line in the lower set of models in their fig. 2. Since their calculation stops at $z = 10$ we extrapolate their black hole mass density curves using a cubic-spline down to $z = 6$. For a Sazonov et al. (2004) type of energy spectrum we obtain SXRB that is about two orders of magnitude lower than the observed one, which is not surprising given that the higher the redshift of the miniquasar is, the less its soft X-ray photons contribute to the observed background. The number of ionizing photons per baryon we obtain is about 10, usually thought to be the minimum number needed to ionize. However, more surprisingly we obtain an optical depth for Thomson scattering of, $\tau \approx 0.075$ which is consistent with the *WMAP* 3rd year results (Page et al. 2006; Spergel et al. 2006). This result is interesting as it shows that for a given black hole evolution history one can satisfy all the observational constraints and ionize the Universe solely with black holes at the same time.

6 SUMMARY

This paper explores the feasibility of heating the IGM with quasars without violating the current observational constraints. Such heating is essential in order to be able to observe the 21-cm emission from neutral hydrogen, prior to and during the epoch of reionization. We have shown that miniquasars with moderate black hole masses can heat the surrounding IGM out to radii of a few comoving Mpc.

In this paper, two Press–Schechter-based black hole mass density evolution scenarios have been proposed, IMBH and SMBH. The first model assumes the black hole population is the end product of pop III stars that leave behind black hole masses of the order of 10–100 $M_{\odot}$. The second model assumes direct formation of black holes as a result of the collapse of low angular momentum primordial haloes. For these two scenarios, we have explored three different quasar spectral templates: a power law with ionization UV radiation, a power law without ionizing UV radiation and a Sazonov et al. (2004) type template.

With the exception of the models that have a 10 per cent duty cycle, we have shown that the quasars are not able to fully ionize the IGM – especially if one assumes the template that does not have ionizing UV photons – while the SXRB constraint is satisfied. We conclude that based on the mass evolution history shown here, there is enough mass in the quasars to heat up the IGM by redshift 15. For example, for quasars with a power-law index of -1 and no ionizing UV radiation, quasars with black hole masses of 10^{3-4} $M_{\odot}$ can heat up the IGM over a $\approx$0.1–1 Mpc comoving radius from the (mini)quasar (see Fig. 5). The models with 6 per cent duty cycle reach such mass per comoving Mpc^3 at redshift larger than 10 for both scenarios.

Curiously, for the black hole mass density evolution, with 10 per cent duty cycle and rigid disc model, proposed by Begelman et al. (2006) we find that this scenario does not violate the SXRB observational constraint and produce about 10 ionizing photons per baryon by $z = 6$, normally thought to be enough to ionize the Universe. We also find that for a model in which the Universe ionizes suddenly at $z = 6$, that this scenario predicts a Thomson scattering optical depth of 0.075, consistent with the *WMAP* 3rd year results.

The main result presented in this paper is ‘good news’ for the new generation of low frequency radio telescopes designed to probe the high-redshift IGM through its 21-cm emission, such as LOFAR, MWA and PAST. It clearly shows that the quasar population could easily decouple the spin temperature from that of the CMB.

However, since the spin temperatures achieved are not very high, this means that the brightness temperature will carry the signature not only of the ionized fraction and density fluctuations, but also of the variations in the spin temperature. This complicates the interpretation of the observed brightness temperature in terms of its link to the cosmological fields. Nevertheless, the high spin temperature bubbles are expected to overlap before those of the ionization, a factor that will mitigate this complication. Furthermore, one can turn this around and argue that these fluctuations will teach us more about the ionizing sources than about cosmology. An extended tail in the spin temperature will be a clear signature of power-law radiation, that is, quasars, while a short tail will be a clear signature of thermal radiation, that is, stars.

ACKNOWLEDGMENTS

JS and NS acknowledge the Kapteyn Astronomical Institute and NS and SZ acknowledge the Department of Astrophysics at Oxford for hospitality. The authors thank A. Ferrara and L. V. E. Koopmans for discussions, A. Nusser for comments on the manuscript and L. Chuzhoy for drawing our attention to the influence of collisional excitations on the spin temperature. The authors thank the anonymous referee for very helpful comments. NS is supported by a Grant-in-Aid for Scientific Research from the Japanese Ministry of Education (No. 17540276).

REFERENCES

Abel T., Bryan G. L., Norman M. L., 2000, ApJ, 540, 39
Abel T., Bryan G. L., Norman M. L., 2002, Sci, 295, 93
Allison A. C., Dalgarno A., 1969, ApJ, 158, 423
Begelman M. C., Volonteri M., Rees M. J., 2006, MNRAS, 370, 289
Bond J. R., Arnett W. D., Carr B. J., 1984, ApJ, 280, 825
Bromm V., Larson R. B., 2004, ARA&A, 42, 79
Bromm V., Loeb A., 2003, ApJ, 596, 34
Bromm V., Coppi P. S., Larson R. B., 2002, ApJ, 564, 23
Chen X., Miralda-Escude J., 2006, preprint (astro-ph/0605439)
Chuzhoy L., Alvarez M. A., Shapiro P. R., 2006, ApJ, 648, L1
Ciardi B., Ferrara A., 2005, Space Sci. Rev., 116, 625
Ciardi B., Madau P., 2003, ApJ, 596, 1
Dijkstra M., Haiman Z., Loeb A., 2004, ApJ, 613, 646
Fan X. et al., 2003, AJ, 125, 1649
Fan X. et al., 2006, AJ, 131, 1203
Field G. B., 1958, Proc. IRE, 46, 240
Field G. B., 1959, ApJ, 129, 551
Haiman Z., Rees M. J., Loeb A., 1997a, ApJ, 484, 985
Haiman Z., Rees M. J., Loeb A., 1997b, ApJ, 476, 458
Heger A., Woosley S. E., 2002, ApJ, 567, 532
Hogan C. J., Rees M. J., 1979, MNRAS, 188, 791
Kuhlen M., Madau P., 2005, MNRAS, 363, 1069
Kuhlen M., Madau P., Montgomery R., 2006, ApJ, 637, L1
Madau P., Meiksin A., Rees M. J., 1997, ApJ, 475, 429
Madau P., Rees M. J., Volonteri M., Haardt F., Oh S. P., 2004, ApJ, 604, 4
Mitsuda K. et al., 1984, PASJ, 36, 741
Moretti A., Campana S., Lazzati D., Tagliaferri G., 2003, ApJ, 588, 696
Nusser A., 2005, MNRAS, 359, 183
O’Shea B., Norman M. 2007, ApJ, 654, 66
Page L. et al., 2006, preprint (astro-ph/0603450)
Pen U.-L., 1999, ApJS, 120, 49
Press W. H., Schechter P., 1974, ApJ, 187, 425
Pritchard J. R., Furlanetto S. R., 2006, preprint (astro-ph/0607234)
Rakavy G., Shaviv G., Zinamon Z., 1967, ApJ, 150, 131
Rhook K. J., Haehnelt M. G., 2006, MNRAS, 373, 623
Ricotti M., Ostriker J. P., 2004a, MNRAS, 350, 539
Ricotti M., Ostriker J. P., 2004b, MNRAS, 352, 547
Rybicki G. B., Lightman A. P., 1979, Radiative Processes in Astrophysics. Wiley, New York
Salvaterra R., Haardt F., Ferrara A., 2005, MNRAS, 362, L50
Sazonov S. Y., Ostriker J. P., Sunyaev R. A., 2004, MNRAS, 347, 144
Schaye J., Theuns T., Rauch M., Efstathiou G., Sargent W. L. W., 2000, MNRAS, 318, 817
Shakura N. I., Sunyaev R. A., 1973, A&A, 24, 337
Sheth R. K., Tormen G., 1999, MNRAS, 308, 119
Shapiro S. L., 2004, in Ho L. C., ed., Coevolution of Black Holes and Galaxies, Carnegie Observatories Astroph. Ser. Cambridge Univ. Press, Cambridge, p. 103

Shull J. M., van Steenberg M. E., 1985, ApJ, 298, 268
Silk J., Goldsmith D. W., Field G. B., Carrasco L., 1972, A&A, 20, 287
Smith F. J., 1966, Planet. Space Sci., 14, 929
Sołtan A. M., 2003, A&A, 408, 39
Spaans M., Silk J., 2006, ApJ, 652, 902
Spergel D. N. et al., 2006, preprint (astro-ph/0603449)
Steinmetz M., Bartelmann M., 1995, MNRAS, 272, 570
Theuns T., Zaroubi S., Kim T.-S., Tzanavaris P., Carswell R. F., 2002a, MNRAS, 332, 367
Theuns T., Schaye J., Zaroubi S., Kim T.-S., Tzanavaris P., Carswell B., 2002b, ApJ, 567, L103
Volonteri M., Rees M. J., 2005, ApJ, 633, 624
Wild J. P., 1952, ApJ, 115, 206
Wouthuysen S. A., 1952, AJ, 57, 31
Yoshida N., Sokasian A., Hernquist L., Springel V., 2003, ApJ, 598, 73
Zaroubi S., Silk J., 2005, MNRAS, 360, L64
Zygelman B., 2005, ApJ, 622, 1356

This paper has been typeset from a TEX/LATEX file prepared by the author.